



Synthesis and study the loading and releasing of losartan potassium on the modified mesoporous silica

Malihe Arhami¹ · Jafar Mahmoudi¹

Received: 25 October 2021 / Accepted: 26 February 2022
© Institute of Chemistry, Slovak Academy of Sciences 2022

Abstract

In this study, the mesoporous MCM-41 have been prepared and modified with acidic agents, including citric acid, acetic acid, and ascorbic acid to obtain a suitable drug carrier for the controlled release of losartan potassium. The prepared samples have been characterized by XRD, FTIR, SEM, TGA and BET methods. Then, the drug loading of losartan potassium on modified MCM-41 has been investigated for the first time. Subsequently, the effects of carrier type, carrier concentration, contact time, drug solution concentration and pH of the drug solution have been investigated, and the optimum loading conditions have been evaluated. The results of drug loading show that loading of losartan potassium in MCM-41 functionalized with citric acid and ascorbic acid is higher than other synthesized samples. The amount of losartan loaded in these carriers is 97.68 and 60.76%, respectively. Moreover, the results of the drug release phase experiments in the pH range of (3–11) show that the highest drug release is at pH = 7.4. Finally, five kinetic models are used to determine the rate of the drug release. Based on the kinetic modeling, it is found that the release of losartan potassium from MCM-41-Ci and MCM-41-As obeys the Higuchi model with non-Fickian diffusion. This was confirmed by investigating the results of error function analysis.

Keywords Mesoporous silica · Controlled drug release · Losartan potassium · Loading

Introduction

Traditional drug delivery systems have virtually no control over the location and speed of drug release. Also, the constant change of the drug concentration in the blood reduces the efficacy of the drug, so the side effects are inevitable. Slow release systems are the initial drug delivery in which the drug is embedded in an appropriate release system and produces uniform concentration of the drug in the blood for a certain period of time. In this method, the type of particle, the way of entering the drug into the body, and the way of releasing the drug are the most important parameters. The type of disease and the type of drug regulate these parameters (Chen et al. 2021). The focus of drug technology is on the getting the drug to the right place in the body, at the right time, and with the desired therapeutic effects. The advantages of this technology include the ability of maintaining the drug concentration at a relatively constant level for a

specified period, adjustable drug release rate depending on the drug delivery site, the ability of delivering multiple medications with one formulation, and the possibility of drug delivery in the nanoscale (Chen et al. 2021; Diaf et al. 2012).

Many materials have been studied as drug release systems, including biodegradable polymeric materials (Diaf et al. 2012; Musial et al. 2010) and ceramic materials such as hydroxyapatite (Pasandideh et al. 2020) and calcium phosphates (Fosca et al. 2022). Recently, the application of mesoporous silica materials (Baumgartner and Planinšek 2021; Deaconu et al. 2018) in slow release systems has drawn much attention. These compounds have very large surface area, and their cavities are adjustable. They also have high level of functionality, so they provide an opportunity for the development of new drug delivery systems to control the rate of drug loading and releasing (Manzano and Vallet-Regí 2010; Wang 2009). In fact, the high porosity of mesoporous silica materials leads to the biologically active molecules with different size to occupy the cavities of these materials. Additionally, the regular porosities of these compounds result in obtaining the appropriate loading and release rate of the drug (Mahmoudi et al. 2015). In recent years, most of the researchers have focused on the studies of the M41S as

✉ Jafar Mahmoudi
mahmoudi@du.ac.ir

¹ School of Chemistry, Damghan University, Damghan, Iran

porous silicate compounds. Three important types of M41S family are MCM-41 with hexagonal structure, MCM-48 with cubic structure, and MCM-50 with layered structure (Popova et al. 2021; Talaei et al. 2021). The diameter of the channels of MCM-41 with regular hexagonal channels can be set in the range of (1.5–10) nm. High surface area, large cavity volume, and ideal biocompatibility make the MCM-41 as one of the best materials to carry many compounds so that it attracts a great deal of attention in the realm of drug delivery systems (Solanki et al. 2019). In the study of drug release, the first step is the absorption of the drug by the carrier. Chemical surface modification of adsorbents such as MCM-41 is known to increase efficiency. Ho et al. (2003), synthesized ordered mesoporous silica adsorbents by grafting amino- and carboxylic-containing functional groups onto MCM-41 for the adsorption of organic dyes. Samson et al. (Akpotu and Moodley 2016) modified MCM-41 with citric acids and used it in the adsorption of cationic dyes. The results indicate the modified sample showed an improved adsorption as compared to the unmodified MCM-41.

On the other hand, losartan is one of the most commonly used drugs. It is also known as one of the angiotensin II receptor blocking drugs. Angiotensin II is responsible for tightening blood vessels in the body. Losartan is used to treat high blood pressure alone or in combination with other antihypertensive drugs. In spite of the wide application of losartan, the losartan release has been reported only in a few literature works: design and evaluation of controlled release losartan potassium microcapsules (Vidyadhara et al. 2013); regulating cancer-associated fibroblasts with losartan-loaded injectable peptide hydrogel to potentiate chemotherapy in inhibiting growth and lung metastasis of triple negative breast cancer (Hu et al. 2017). Therefore, further investigation into the controlled-release of losartan potassium is necessary. Also, as mentioned above, it seems that mesoporous silica materials such as MCM-41 have important advantages that can be tailored to control the diffusion rate of an adsorbed losartan potassium. Based on our finding, the application of mesoporous MCM-41 modified with citric acid, acetic acid, and ascorbic acid as drug carrier for the controlled release of losartan potassium has yet to be studied.

In this work, the MCM-41 has been synthesized and then modified with ascorbic, acetic and citric acids. The samples have been characterized with XRD, FTIR, SEM, TGA and BET techniques. The loading and releasing experiments with losartan potassium on synthesized samples were performed. The effect of different variables on loading and releasing of losartan such as carrier type, reaction time, carrier weight, pH of drug solution, drug concentration at drug loading stage, pH of phosphate buffer solution, and the time of the drug release stage have been studied. Moreover, the kinetics of losartan release has been studied by using different

kinetic models, and the best kinetic model and parameters have been obtained.

Experimental

Materials used

Materials that are used for the synthesis of mesoporous MCM-41 samples were CTAB (cetyl trimethyl ammonium bromide) (Merck, Germany) with a purity of 98%, sodium silicate (Merck, Germany) made up of Na₂O in the range of (7.5–8.5) wt% and SiO₂ in the range of (25.5–28.5) wt%, ethanol (Merck, Germany) with a purity of 99% and ammonia with a purity of 25% (Qatran Chemical Company, Iran). The acids used in modification and activation of mesoporous were hydrochloric acid (Sigma-Aldrich) with a purity in the range of (36.5–38.0)%, ascorbic acid (99%, Merck) and citric acid (99.5%, Merck) and acetic acid (Qatran Chemical Company, Iran) with a purity of 99%. Losartan potassium with a purity of 100.0% (Damavand Drug Factory, Iran) and monosodium phosphate and disodium phosphate also used in load and release experiments.

Synthesis of MCM-41

To prepare MCM-41, the specified amount of CTAB and 120 ml of distilled water were mixed under vigorous stirring in a balloon, CTAB was dissolved in the water at the room temperature. Then, 10.25 ml of ammonia solution was added to the initial solution under vigorous mixing by a magnet stirrer. After constant stirring for 30 min, 10 ml of ethanol was added to the above solution and stirred for 30 min. Finally, 7.5 ml of sodium silicate was added to the solution and stirred for 1 h. The resulting sample was filtered, and the precipitate was washed several times with distilled water for neutralizing. Then, it was dried in oven at the temperature of 110 °C for 24 h. The resulting powder was calcined in a furnace at the temperature of 550 °C for 5 h (Parida et al. 2012).

Modification of MCM-41 with various acids

Ascorbic, citric and acetic acids were used to modify the mesoporous silica. To achieve this aim, 1 g of synthesized sample was mixed with 20 ml of 0.6 M acid in an ultrasonic bath for 45 min. The mixture was stirred with a stirrer for 45 min. The mixture was dried in the oven at the temperature of 50°C for 24 h. After 24 h, the oven temperature was increased up to 120°C. The temperature of this step was maintained at 120 °C for 90 min. The obtained precipitate was washed with distilled water until the pH of the washing became neutral. In the final step, the precipitate was dried in the oven at the temperature of 70 °C for 70 h (Kushwaha et al. 2014a). This method was

performed for modification of MCM-41 with three acids. The MCM-41 sample that modified with ascorbic acid, acetic acid and citric acid, were labelled MCM41-As, MCM-41-Ac and MCM-41-Ci, respectively.

Characterization of synthesized samples

The low angle ($2\theta = 1.5 - 10$) and long range ($2\theta = 5 - 80$) X-ray diffraction (XRD), D8-Advance Bruker Cu K α ($\lambda = 0.15406$ nm), was used to determine the structure of the prepared samples. The chemical properties and surface functional groups of the prepared composites were evaluated using a Fourier transform infrared spectroscopy (FT-IR), RXI, manufactured by Perkin Elmer Company. The morphology of the particle surface was also examined using Field Emission Scanning Electron Microscopes (FE-SEM), HTACHI S-4160, with magnification of 20–30,000 and maximum voltage of 30 kV. Besides, in order to examine the thermal stability of the particles, Thermogravimetric analysis (TGA) device, BAHR thermo Analyse STA 503, was used at temperature range of 25–800 °C, 10 °C per minute. Surface area and pore size of the samples were measured using a N₂ adsorption–desorption method at liquid nitrogen temperature (76.03 K) by ASAP 2010 instrument. Prior to the measurements, the sample was degassed at 573 K under vacuum for 5 h.

Drug loading experiments

For loading the drug on different carriers, 0.25 g of the prepared carrier was dispersed into 25 ml of losartan solution (0.5 mg/ml) and stirred with an electric shaker for 24 h in the absence of light. Then obtained powder centrifuged and the supernatant was collected for using in the release experiment. The amounts of losartan adsorbed were determined based on the difference between the initial and remaining concentrations of losartan solution via UV–vis spectroscopy as follows:

$$\text{loading efficiency} \left(\frac{W}{W} \% \right) = \frac{\text{initial amount of losartan} - \text{residual losartan}}{\text{initial amount of drug}} \times 100 \quad (1)$$

Drug release experiments

To determine the amount of drug released from the drug-carrier system, 0.15 g of the losartan-loaded carrier was dispersed in 30 mL of phosphate buffer (pH = 7.4). The resulting suspension was incubated at 37 °C under shaking during 2–48 h in the absence of light. After this step, the sample was withdrawn and centrifuged. Then, the released losartan was monitored by UV–Vis analysis.

Description of the kinetic models

The kinetics of drug release have been studied by using different kinetic models, and the best correlation pattern can be obtained by studying and comparing drug release with different models and choosing the model with the highest correlation coefficient. The investigated kinetic models include the zero-order kinetic model, the first-order model, the Higuchi model, the Korsmeyer-Pepas model and the Hixson-Crowell model (Vilaça et al. 2013).

Zero-order kinetic model is stated as follows.

$$Q_t = Q_0 + k_0 t \quad (2)$$

where Q_t is the percentage of drug released, Q_0 is the initial amount of drug in the solution (most times, $Q_0 = 0$), t is the release time and k_0 is the zero order release constant.

In the first-order kinetic model, the rate of drug release depends on the concentration of drug remaining in the medium at any one time and it is expressed by the following equation:

$$\ln Q_t = \ln Q_0 + k_1 t \quad (3)$$

where k_1 is the first order release constant.

The third kinetic model, Higuchi model, is stated as follows:

$$Q_t = k_H t^{1/2} \quad (4)$$

In this model, the size of the particles is a significant factor. Also, k_H shows the rate constant.

The Korsmeyer-Papas model can be written as follows:

$$Q_t = k_p t^n \quad (5)$$

The main assumption of this equation is the controlled infiltration of the polymer substrate. In this model, n determines the type of infiltration, k_p is the rate constant. In drug release from polymer matrices, various factors such as the penetration of liquid into the matrix body, the hydration,

polymer ablation and gelation, the diffusion, and diffusion of drug molecules through the gel and polymer dissolution are involved. The mechanism of drug release in these cases follows the Korsmeyer-Peppas equation, also known as the power law.

The other kinetic model, Hixson Crowell, is expressed as follows.

$$Q^{1/3} - Q_0^{1/3} = K_C \times t \quad (6)$$

This model examines drug release from systems in which changes in surface area and particle thickness exist. K_C is the Hixson–Crowell constant.

Results and discussion

Characterization of the synthesized samples

XRD investigation

Figure 1 shows the XRD patterns of MCM-41 and modified MCM-41 with various acids. Figure 1a is the XRD pattern of the synthesized sample in the 2θ range of $(1.5–10)^\circ$. The powder X-ray diffraction patterns of MCM-41 samples show three peaks corresponding to indices, including (100), (110), and (200) at 2θ between 0 and 5, showing the characteristic of the high order of the meso-material. In the present study, the XRD spectra obtained for synthesized MCM-41 are compatible with XRD spectra of different literature works (Idris et al. 2011; Mannaa et al. 2021). In the samples modified with various acids, the (110) and (200) peaks disappear and one peak near (100) peak appears with a reduction in the intensity of the peak which indicates a reduction in the structural order of the modified samples, especially for MCM-41 modified with ascorbic acid a reduction in the intensity of the peak is significant. It seems that the presence of cyclic groups in the structure of ascorbic acid increases the interaction between these groups and pore of MCM-41 other than citric acid and acetic acid. In addition, the decrease in peak intensities is due to the decrease in pore space as a result of

interaction between acid groups and MCM-41. Figure 1b shows the wide angle XRD images for the MCM-41 and modified specimens obtained in the range of $(4–80)^\circ$. For all samples, a large amorphous peak around $(20–30)^\circ$ in the XRD pattern is the characteristic of siliceous material. In the modified specimens, no significant characteristic peak of acid species is found in the corresponding XRD patterns.

FT-IR analysis

Figure 2 shows the FT-IR spectra of MCM-41 and modified MCM-41 with different acids. A relatively high peak observed in the 3400 cm^{-1} can be attributed to the stretching vibration of the OH group and the water absorbed on the sample surface. Moreover, the band at 1556 cm^{-1} in MCM-41 can be ascribed to C=O stretching vibration (Hayemasae et al. 2020). The same band appears in the spectra of acid functionalized MCM-41 matrix but with higher intensity that indicates a chemical interaction occurred between carboxylic acid of ascorbic, citric and acetic acids, and surface groups of MCM-41. Also, the peak at 1416 cm^{-1} can be attributed to the CH_2 scissor vibration (Monash and Pugazhenti 2010). Increase in the mentioned peak intensity in the acid functionalized MCM-41 matrix confirms the binding of carboxylic groups to the MCM-41 matrix. The absorption peak observed around 1080 and 798 cm^{-1} is due to asymmetric and symmetric stretching of Si–O–Si, respectively (Mannaa et al. 2021). Also, the absorption peak observed at 464 cm^{-1} can be attributed to the bending vibrations of the siloxane group (Si–O–Si) in the silicate compressed lattice (Kushwaha et al. 2014b).

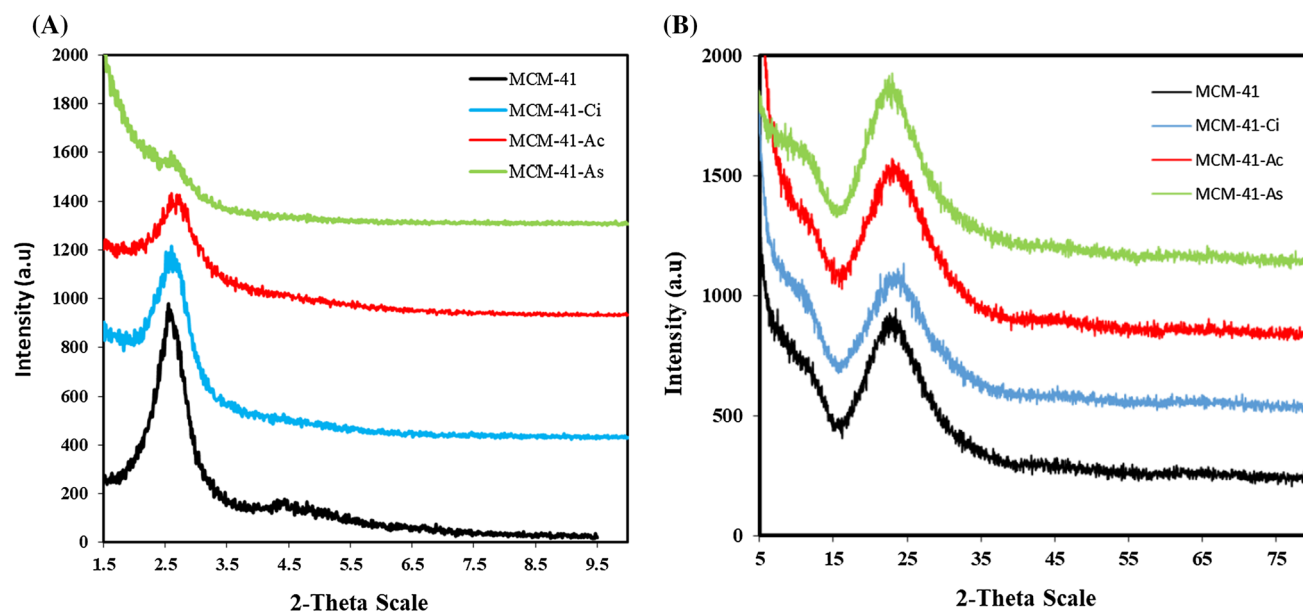


Fig. 1 X-ray diffraction patterns for synthesized samples. a Low-angle, b Wide-angle

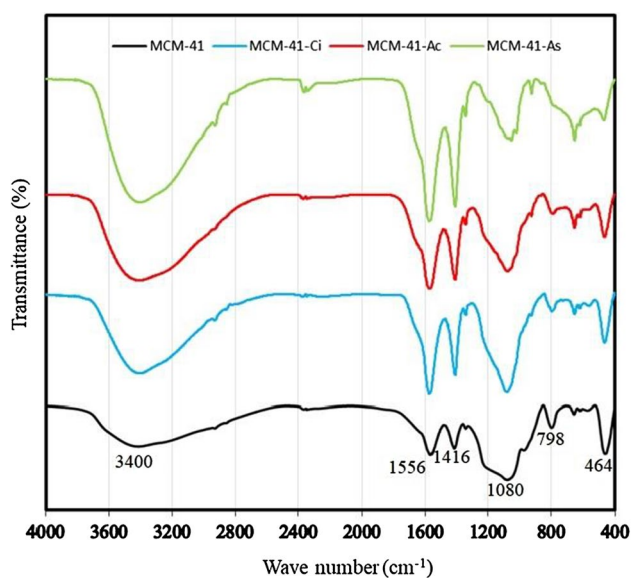


Fig. 2 FT-IR spectra of synthesized samples

SEM analysis

Figure 3a–d shows SEM images of the MCM-41, MCM41-Ci, MCM-41-Ac and MCM-41-As, respectively. There is a considerable change between these samples. The morphological appearance of MCM-41 comprised a mixture of rods and amorphous particles and converted to the spheres and rods in the modified form of MCM-41 especially in the MCM41-Ci and MCM-41-As samples. An enlarged view of MCM41-Ci and MCM-41-As samples, SEM images revealed coating by mentioned acid as it is visible on small grain like spheres of MCM-41 particles. Based on the micrographs, it was found that the ascorbic and citric acids were dispersed in the mesoporous MCM-41 network. It means that these acids have a good synergism with MCM-41 and improve its network which may be promising approach for drug adsorption and release.

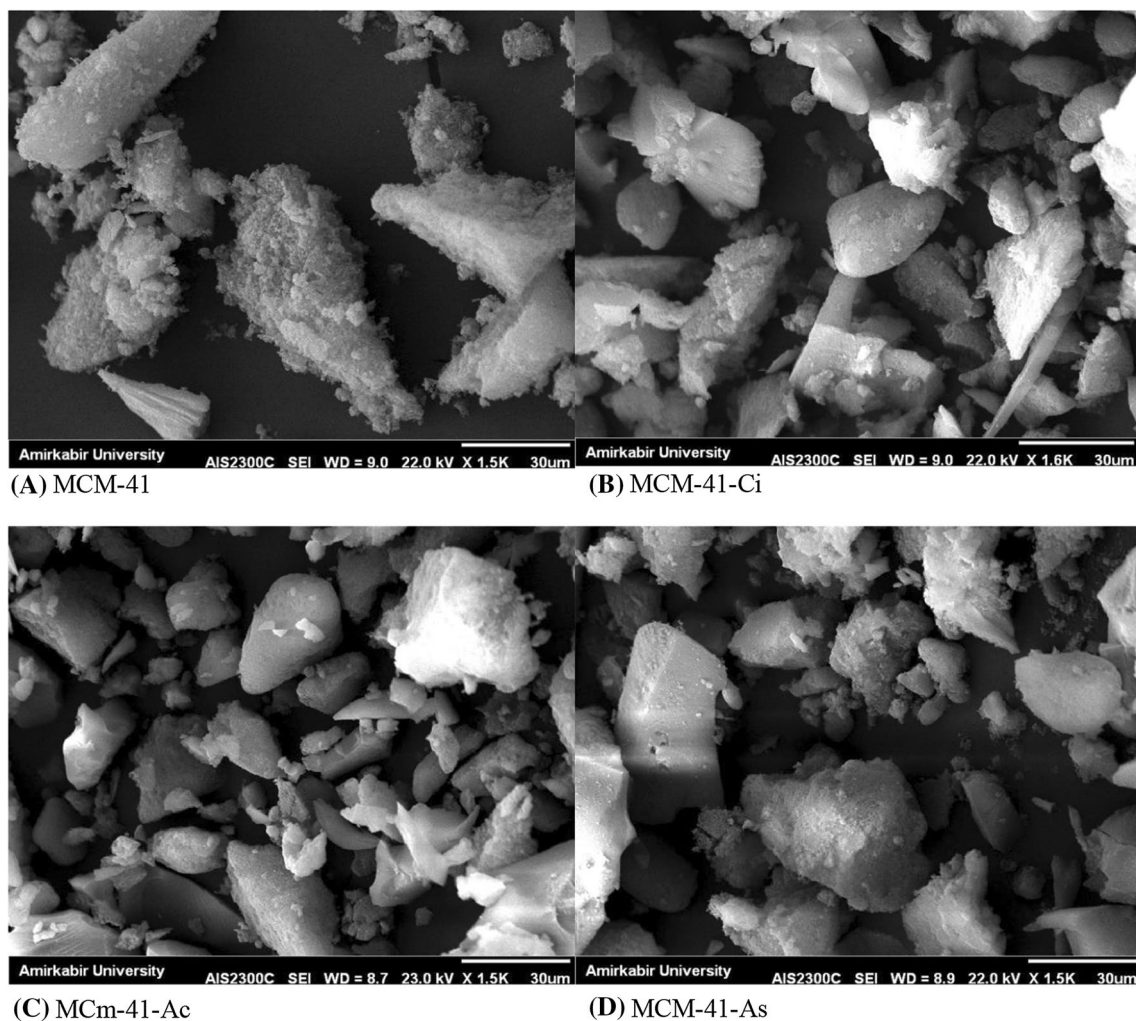


Fig. 3 SEM images of synthesized samples

TGA analysis

Figure 4 shows TGA/DTA curves for MCM41-Ci and MCM-41-As before and after the absorption of Losartan in the temperature range of (20–800)°C. The MCM41-Ci results in the first weight loss (about weight percent of 9) that occurs at the temperature range of (0–120)°C. This can be due to the loss of adsorbed water molecules. The second weight loss (about 4wt%) occurs at the temperature range of (300–450)°C that can be attributed to the carrier decomposition. In the TGA thermograms of

MCM41-Ci/Lo (Losartan), the second step around 400 °C can be attributed to the decomposition and oxidation process of the Losartan, proving its presence in the composite (about 8.5wt. %) (Zendehdel et al. 2014). The similar trend was obtained for the TGA thermograms of MCM-41-As before and after absorption of losartan. It was observed that both the MCM-41-As and MCM-41-As-Lo show sluggish decomposition, however, the weight loss in case of MCM-41-As-Lo (about 11.8 wt%) is higher than that of MCM-41-As (about 6.5 wt%) in the temperature range of (300–450)°C which indicate the presence of losartan

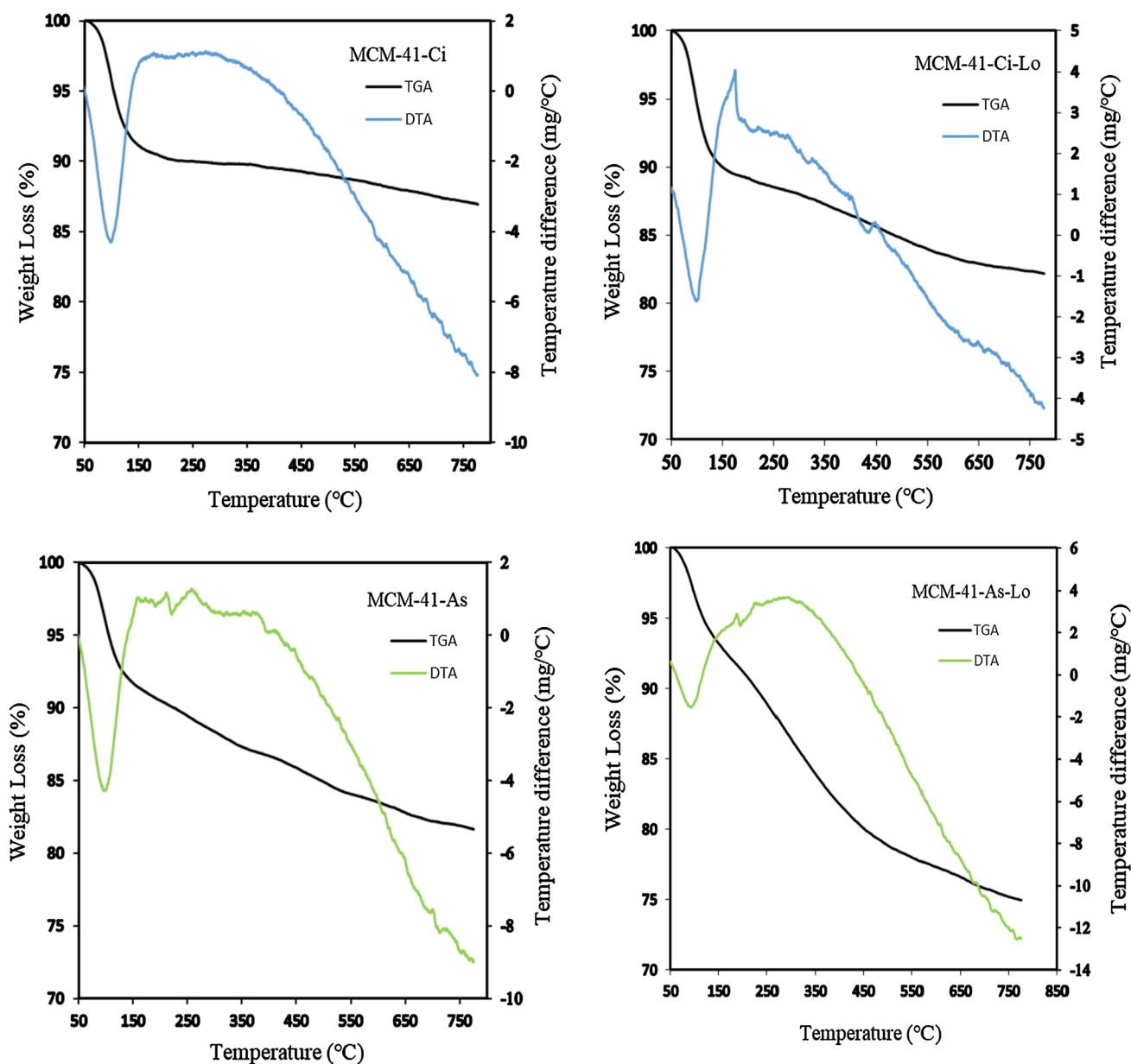


Fig. 4 TGA thermograms of MCM41-Ci and MCM-41-As before and after absorption of Losartan

in the composite (Zendehdel et al. 2014; Soenmez et al. 2018). Furthermore, at 800 °C, the residue for MCM41-Ci/Lo (82%) was found to be higher in comparison with MCM-41-As-Lo (75%). The higher residue of MCM41-Ci/Lo confirms its higher thermal stability than the MCM-41-As-Lo.

BET analysis

The nitrogen adsorption/desorption isotherms of the prepared MCM-41, MCM41-Ci and MCM-41-As are shown in Fig. 5. Based on Fig. 5, for all samples, a distinctive type IV adsorption isotherm for mesoporous solids was observed that indicating the mesoporous nature of the synthesized samples. For the determination of the surface area and the pore size distribution, the BET and BJH (Barrett-Joyner-Halenda) methods were used, respectively. The high BET surface area of the samples including MCM-41, MCM41-Ci and MCM-41-As was obtained 802, 594 and 573 m² g⁻¹, respectively, that coincided with the high surface area of mesoporous materials (Akpotu and Moodley 2016). The results indicated that modification of MCM-41 with citric and ascorbic acids caused a reduction in surface area. This was as a result of pore filling by citric and ascorbic acids. The pore diameter of samples was obtained 22.28, 26.14 and 24.09 Å for MCM-41, MCM41-Ci and MCM-41-As, respectively, that agreed with the range of pore diameter for mesoporous materials (Monash and Pugazhenth 2010).

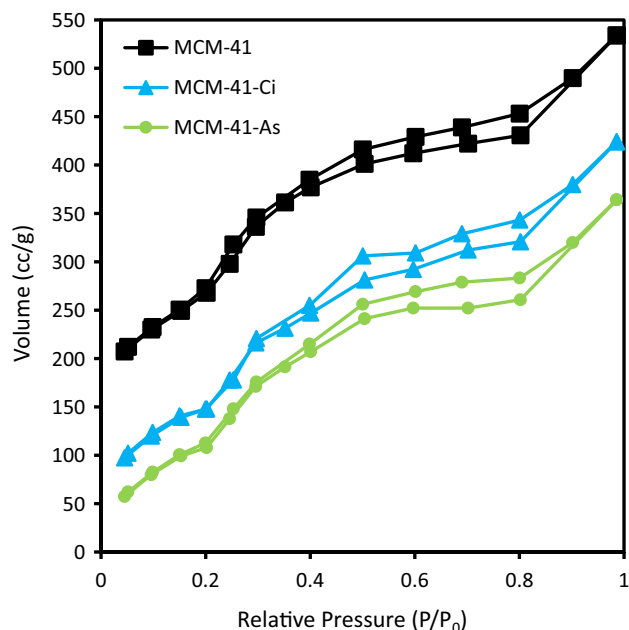


Fig. 5 Nitrogen adsorption/desorption isotherm of the MCM-41, MCM-41-Ci and MCM-41-As

Drug loading studies

The effect of carrier type on drug loading

Losartan is in the drug class angiotensin receptor blockers, and it has been used as a model molecule to evaluate the capacity of prepared MCM-41, MCM41-Ci, MCM-41-Ac, and MCM-41-As in controlled release of drug molecules. The drug loading efficiency of carrier samples is illustrated in Fig. 6. One can see in Fig. 6 that the highest loading efficiency is for MCM-41-Ci (about 74.27%) and MCM41-As (equal to 49.82%).

The effect of carrier concentration on drug loading

The amount of the carrier concentration is an important issue in drug absorption. Figure 7 shows effects of carrier concentration. According to Fig. 7, for both selected carriers, 0.25 g of carrier leads to achieving 68.9 and 53.1% of the drug adsorption for MCM-41-Ci and MCM-41-As, respectively. This result shows the higher adsorption percentage than the other conditions; therefore, 0.25 g was selected as the optimum carrier weight. In fact, when the amount of carrier increases, the available sites for contact increase and much more drug can absorb on the carrier surface. In contrast, at higher carrier concentration, some carrier particles tend to become condensed. This results in decreasing the number of active or accessible surface sites and the amount of drug absorption reduces.

The influence of contact time on drug loading

Due to the equilibrium nature of the adsorption process, the contact time is very important to achieve the equilibrium.

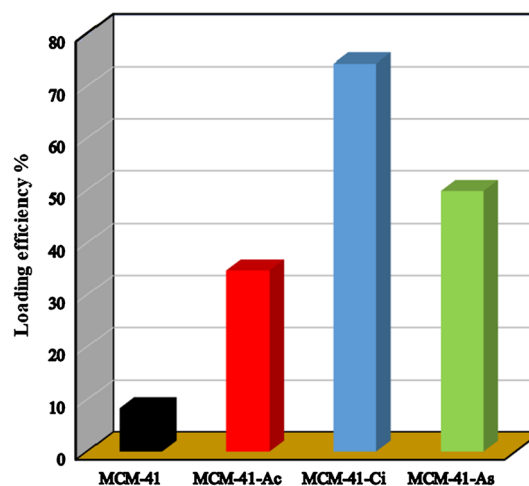


Fig. 6 Compression between different synthesized samples on loading of losartan potassium

Fig. 7 The effect of carrier amount on drug loading

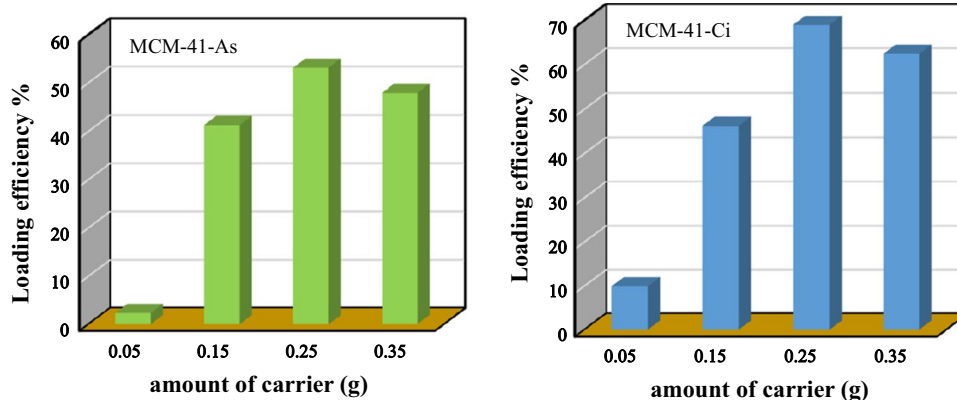
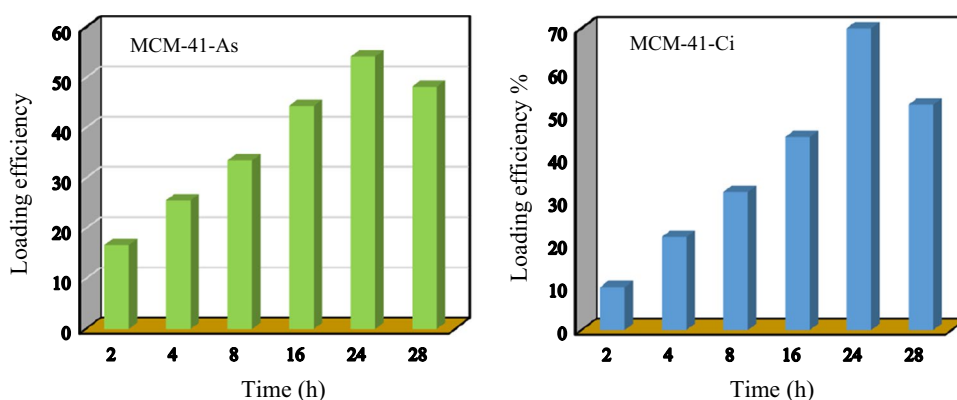


Fig. 8 Effect of time contact on the drug loading at MCM-41-As and MCM-41-Ci carrier



Therefore, the optimized carrier's amount was in contact with losartan at different times. The results of the experiments are shown in Fig. 8. Experimental results show that drug loading increases when contact time increases from 2 to 24 h. During this period of time, the active sites of the carriers used are gradually occupied and eventually saturated for 24 h. It is possible that some molecules of the absorbed drug tend to be desorbed. Therefore, at longer exposure times of 24 h, the rate of drug loading is reduced. Therefore, the contact time of 24 h is selected as the optimum time in the drug loading phase.

Effect of drug concentration on loading rate

The effect of different concentrations of losartan potassium was investigated in suspensions containing 0.25 g of carrier in 25 ml losartan solution for 24 h contact time. Table 1 shows the results of losartan loading at various concentration experiments. According to the results of Table 1, low adsorption exists at very low or very high concentrations of drug. According to the results, by increasing the concentration of losartan up to 0.5 mg/ml, the uptake of drug

Table 1 The performance of carriers for adsorption of losartan at various concentration of losartan

losartan concentration (mg/ml)	Loading efficiency (%)	
	MCM-41-As	MCM-41-Ci
0.1	14.538	53.359
0.3	19.62	75.36
0.5	20.611	98.492
0.7	13.978	28.268
0.9	10.995	14.591

Conditions: dosage of carrier: 10 g/l; pH: 10; adsorption time: 24 h

increases until all available pores of carrier are filled by losartan and the carrier surface is saturated. After a certain concentration (0.5 mg/ml), the amount of adsorption decreases. Apparently, at concentrations above 0.5 mg/ml, the hydrogen bonding occurred between the losartan molecules and dimer-like molecules with higher size formed. Therefore, these larger molecules do not enter the surface, and the carrier pores and the drug adsorption are reduced.

Influence of pH of drug solution on loading

In this section, the effect of the pH of the losartan solution in the range of (3–11) was investigated on adsorption efficiency. Table 2 presents the results of this part. According to these results, the neutralized pH of the losartan solution increases the amount of the drug absorbed by the carriers. For both carriers, when the pH of drug solution equal to 7, the best performance of the adsorption was obtained.

Drug release studies

The effect of phosphate buffer on drug release rate

In order to optimize the pH of the buffer during the drug release phase, five experiments were designed in which all conditions were the same, but the pH of the phosphate buffer solution was changed to 2, 4, 7.4, 9 and 11 in each experiment to obtain the optimum pH. Figure 9 shows the effect of pH of the buffer solution on the release of losartan. One can see that the pHs below 7.4 increase the amount of drug released for both carriers when the pH of the solution

Table 2 The performance of carriers for adsorption of losartan at various pH of losartan solution

pH of solution	Loading efficiency (%)	
	MCM-41-As	MCM-41-Ci
3	32.816	6.649
5	35.409	91.012
7	60.76	97.624
9	10.134	31.411
11	10.11	3.772

Conditions: dosage of carrier: 10 g/l; losartan concentration: 0.5 mg/ml; adsorption time: 24 h

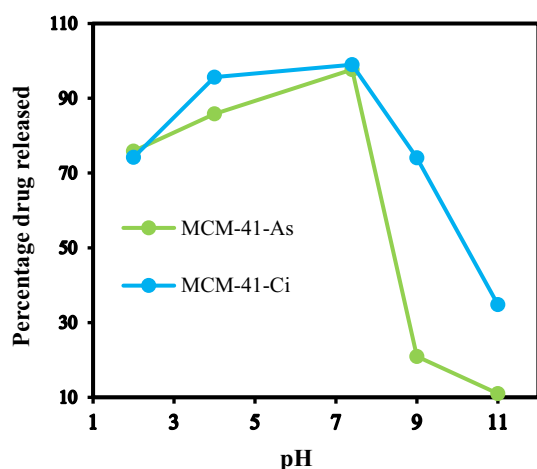


Fig. 9 Effect of pH on drug release on MCM-41-As and MCM-41-Ci

increases. When the pH of phosphate buffer solution is 7.4, carriers have a better performance in the drug release phase and they have the highest drug release rate. Under alkaline conditions ($\text{pH} > 7.4$), increasing the pH leads to forming an ionic group of losartan that absorbs the carrier; therefore, it decreases the amount of the released drug. Finally, it is found that when the pH of the phosphate buffer solution is 7.4, the highest release rate of the drug can be obtained.

The effect of time on the drug release

To test the effect of time on the drug release, experiments were designed and performed in 2, 4, 6, 10, 16, 18, 20 and 24 h. The release of the drug in the delivery process can be conducted as follows. At the beginning of the drug release, the fluid must penetrate into the pores on the carrier surface. Then, the fluid penetrates into the internal pores of the carrier, and the drug is dissolved in the fluid. Finally, since the fluid dissolves the drug, it removes the drug from the carrier/drug system. Figure 10 shows the amount of losartan release over time at $\text{pH} = 7.4$. The rapid release of the drug that occurs during the early stages of release can be attributed to the release of a drug that mainly accumulates on the outer edges of the carrier. However, most drugs are stored in the main carrier pores (internal pores), for which a long time is required for dissolving and releasing the drug from these main cavities. After releasing most of the drugs, a small amount of drugs are released on the walls of the carrier pores.

The results of the kinetic model

As mentioned in the previous section, five kinetic models have been applied to this study. To recognize the appropriate

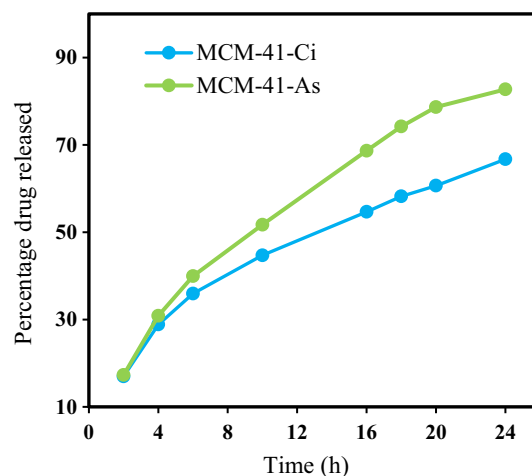
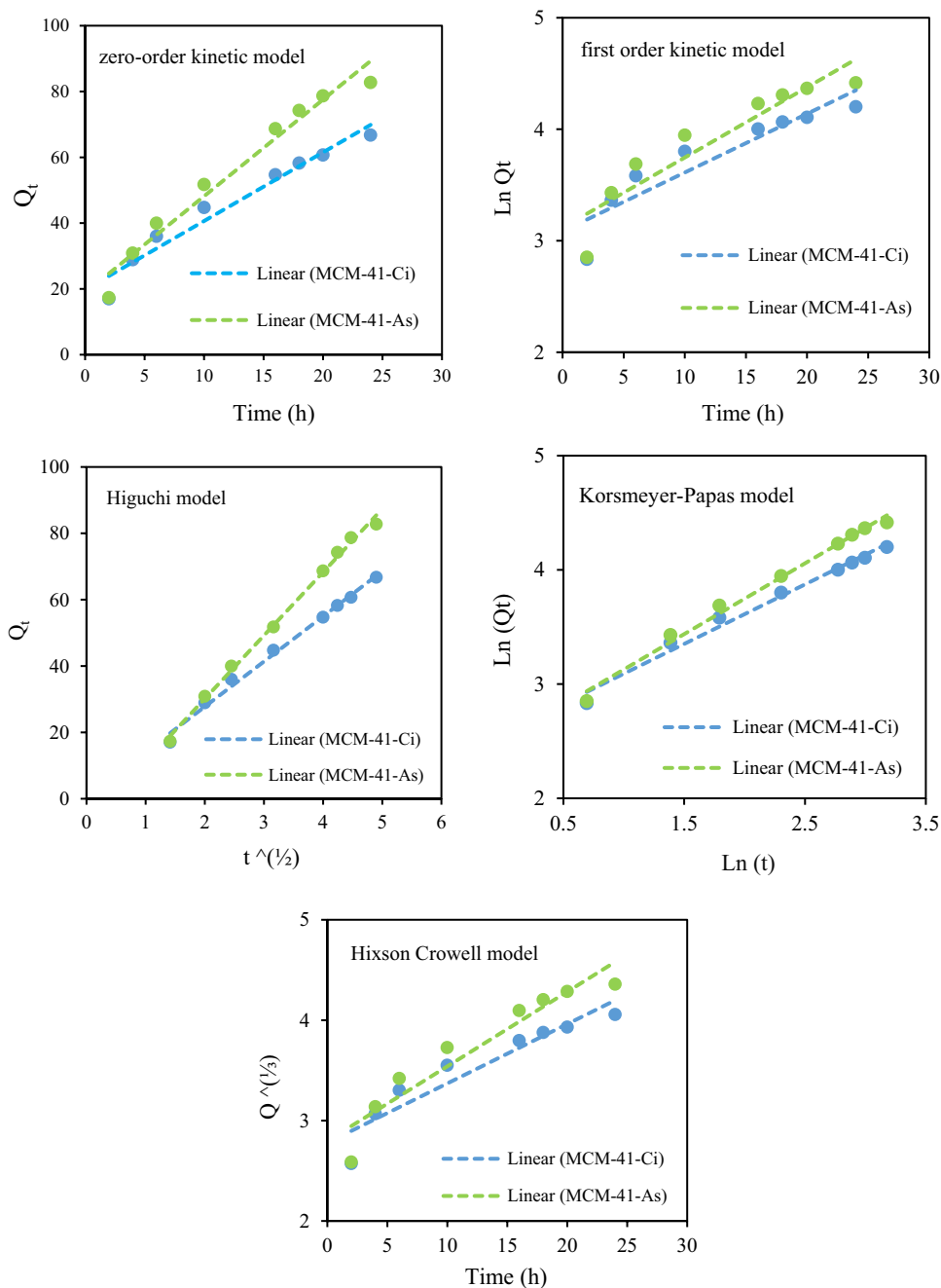


Fig. 10 Time-diagram on drug release on MCM-41-As and MCM-41-Ci

Fig. 11 The kinetics of drug release with different models



kinetic model and mechanism of drug release, the parameters of each kinetic model have been determined based on the experimental kinetic data. Figure 11 shows the release of losartan potassium from carriers of MCM-41-Ci and MCM-41-As by different kinetic models at pH=7.4. The constants determined by the kinetic models are given in Table 3.

Based on the obtained correlation coefficients, it is fully apparent that the release of losartan potassium from MCM-41-Ci and MCM-41-As carriers follows the Higuchi model. According to this model, the liquid penetrates the carriers of MCM-41-Ci and MCM-41-As matrix and dissolves the embedded losartan, and so the losartan release seems to be a

Table 3 The kinetic parameters of all applied models in the present study

Kinetic model	Parameter	MCMC-41-Ci	MCM-41-As
Zero order	k_0	2.088	2.937
	R^2	0.956	0.966
First order	k_1	0.053	0.063
	R^2	0.848	0.862
Higuchi	k_H	13.608	19.074
	R^2	0.993	0.996
Korsmeyer-Peppas	k_p	13.067	12.284
	n	0.521	0.620
	R^2	0.985	0.990
Hixson Crowell	k_c	0.059	0.074
	R^2	0.892	0.907

Table 4 Error functions to evaluate the fit of the linear equation

Error functions	Equation
Residual root mean square error	$RMSE = \sqrt{\frac{1}{N} \sum_{i=1}^N (y_{exp} - y_{cal})^2}$
The variance accounted for	$VAF = \left[1 - \frac{\text{var}(y_{exp} - y_{cal})}{\text{var}(y_{exp})} \right] \times 100$
Mean absolute percentage error	$MAPE = \frac{1}{N} \sum_{i=1}^N \left \frac{y_{exp} - y_{cal}}{y_{cal}} \right \times 100$
Mean absolute error	$MAE = \frac{1}{N} \sum_{i=1}^N y_{cal} - y_{exp} $
Mean squared error	$MSE = \frac{1}{N} \sum_{i=1}^N (y_{cal} - y_{exp})^2$
The coefficient of determination	$R^2 = 1 - \frac{\sum_{i=1}^N (y_{cal} - y_{exp})}{\sum_{i=1}^N (y_{cal} - y_m)}$
The correlation coefficient	$R = \frac{\text{Mean}[(y_{exp} - \text{mean}(y_{exp})) (y_{cal} - \text{mean}(y_{cal}))]}{(\sigma_{y_{exp}})(\sigma_{y_{cal}})}$
Non-linear chi-square	$\chi^2 = \sum_{i=1}^N \frac{(y_{cal} - y_{exp})^2}{y_{exp}}$
The sum of square of the error	$SSE = \sum_{i=1}^N (y_{exp} - y_{cal})^2$
The sum of the absolute error	$SAE = \sum_{i=1}^N y_{cal} - y_{exp} $
Average relative error	$ARE = \frac{1}{N} \sum_{i=1}^N \left \frac{y_{cal} - y_{exp}}{y_{exp}} \right $

process predominately controlled by diffusion. According to the results, the Korsmeyer–Peppas model can also be considered as a suitable kinetic model, and since the “n” value (diffusion exponent) in this model is in the range of 0.45–0.89, we can conclude that the losartan release was anomalous (non-Fickian) transport. Similar drug release kinetics were

reported for nanoparticles by Bhandari (Bhandari et al. 2017) and Lu (Lu and Hagen 2020).

Error function analysis was done to verify the models for the kinetics study. All of the error function equations are listed in Table 4 (İlbay et al. 2017). Table 5 shows the results of error functions for various kinetic models.

Based on error function analysis, the best curve fitting is corresponding to the lower error function value (Rafati et al. 2016). Based on Table 5, a comparison of error functions reflects that Higuchi and Korsmeyer–Peppas model have good correlation with experimental values for the present kinetic study of the release of losartan potassium from MCM-41-Ci and MCM-41-As carriers. These kinetic models give the highest correlation and the lowest values for most of error functions.

Conclusions

In this study, the mesoporous MCM-41 modified with citric acid, acetic acid, and ascorbic acid was used as a carrier for the losartan potassium drug. Firstly, the effect of mesoporous silica and its modified forms with different acids on absorption and release of losartan was investigated. The effect of the type of environment on the acidity or alkalinity, the reaction time, and the amount of drug release was also tested. The results of experiments in this study showed that MCM-41 modified with citric and ascorbic acids had better absorption of losartan potassium than other synthesized samples and unmodified MCM-41. Optimization of the effective variables such as carrier type, carrier amount, contact time, losartan concentration, and pH of solution for drug adsorption step was performed. The optimum variables in the adsorption of losartan with the synthesized carriers were contact time of 24 h, 0.25 g of carrier, pH = 7 and 0.5 mg/ml concentration of drug solution. After performing the adsorption test under the optimum conditions, the percentages of drug absorption by MCM-41-Ci and MCM-41-As carriers were 97.6 and 60.76% and amounts of drug released from system were 57.2 and 79.1%, respectively. Also, after the release tests, the results showed that the amount of drug released depends on the contact time and pH of the solution. Most drug release from drug-carrier system occurs at pH = 7.4. Based on the kinetic modeling, it is found that the release of losartan potassium from MCM-41-Ci and MCM-41-As obeys the Higuchi model that is verified by the results of error function analysis.

Table 5 Kinetics error function data related to the release of losartan potassium from MCM-41-Ci and MCM-41-As carriers

Error function	Kinetic model									
	Zero order		First order		Higuchi		Korsmeyer-Pepas		Hixson Crowell	
	A	B	A	B	A	B	A	B	A	B
RMSE	3.527	4.165	6.007	9.067	1.393	1.427	1.691	2.296	4.870	6.872
VAF	95.609	96.635	86.298	84.052	99.263	99.605	98.917	98.982	91.007	90.850
MAPE	8.876	8.094	13.177	14.928	3.898	2.949	4.457	3.750	11.209	12.237
MAE	2.987	3.487	5.153	7.244	1.086	1.248	1.582	1.585	4.198	5.640
MSE	12.443	17.348	36.091	82.216	1.941	2.036	2.860	5.269	23.714	47.227
R^2	0.956	0.966	0.848	0.862	0.993	0.996	0.984	0.990	0.892	0.907
R	0.856	0.860	0.825	0.820	0.872	0.873	0.871	0.871	0.838	0.838
χ^2	3.607	4.454	7.689	12.583	0.664	0.362	0.667	0.788	5.927	8.645
SSE	99.544	138.78	288.73	657.73	15.530	16.288	22.880	42.158	189.715	377.815
SAE	23.9	27.896	41.222	57.949	8.691	9.984	12.656	12.681	33.583	45.118
ARE	0.095	0.095	0.141	0.162	0.039	0.029	0.044	0.038	0.123	0.137

MCM-41-Ci (A), MCM-41-As (B)

Acknowledgements The authors would like to thank the School of Chemistry, Damghan University, Damghan, Iran, for financing this project.

Declaration

Conflict of interest On behalf of all authors, the corresponding author states that there is no conflict of interest.

References

- Akpotu SO, Moodley B (2016) Synthesis and characterization of citric acid grafted MCM-41 and its adsorption of cationic dyes. *J Environ Chem Eng* 4(4):4503–4513. <https://doi.org/10.1016/j.jece.2016.10.016>
- Baumgartner A, Planinšek O (2021) Application of commercially available mesoporous silica for drug dissolution enhancement in oral drug delivery. *Eur J Pharm Sci* 167:106015. <https://doi.org/10.1016/j.ejps.2021.106015>
- Bhandari J, Mishra H, Mishra PK, Wimmer R, Ahmad FJ, Talegaonkar S (2017) Cellulose nanofiber aerogel as a promising biomaterial for customized oral drug delivery. *Int J Nanomed* 12:2021. <https://doi.org/10.2147/IJN.S124318>
- Chen Q, Li X, Xie Y, Hu W, Cheng Z, Zhong H, Zhu H (2021) Alginate-azo/chitosan nanocapsules in vitro drug delivery for hepatic carcinoma cells: UV-stimulated decomposition and drug release based on trans-to-cis isomerization. *Int J Biol Macromol* 187:214–222. <https://doi.org/10.1016/j.ijbiomac.2021.07.119>
- Deaconu M, Nicu I, Tincu R, Brezoiu AM, Mitran RA, Vasile E, Berger D (2018) Tailored doxycycline delivery from MCM-41-type silica carriers. *Chem Pap* 72(8):1869–1880. <https://doi.org/10.1007/s11696-018-0457-z>
- Diaf K, El Bahri Z, Chafi N, Belarbi L, Mesli A (2012) Ethylcellulose, polycaprolactone, and eudragit matrices for controlled release of piroxicam from tablets and microspheres. *Chem Pap* 66(8):779–786. <https://doi.org/10.2478/s11696-012-0191-x>
- Fosca M, Rau JV, Uskoković V (2022) Factors influencing the drug release from calcium phosphate cements. *Bioact Mater* 7:341. <https://doi.org/10.1016/j.bioactmat.2021.05.032>
- Hayeemasae N, Senseem Z, Surya I, Sahakaro K, Ismail H (2020) Synergistic effect of maleated natural rubber and modified palm stearin as dual compatibilizers in composites based on natural rubber and halloysite nanotubes. *Polymers* 12(4):766. <https://doi.org/10.3390/polym12040766>
- Ho KY, McKay G, Yeung KL (2003) Selective adsorbents from ordered mesoporous silica. *Langmuir* 19(7):3019. <https://doi.org/10.1021/la0267084>
- Hu C, Liu X, Ran W, Meng J, Zhai Y, Zhang P, Li Y (2017) Regulating cancer associated fibroblasts with losartan-loaded injectable peptide hydrogel to potentiate chemotherapy in inhibiting growth and lung metastasis of triple negative breast cancer. *Biomaterials* 144:60–72. <https://doi.org/10.1016/j.biomaterials.2017.08.009>
- Idris SA, Harvey SR, Gibson LT (2011) Selective extraction of mercury (II) from water samples using mercapto functionalised-MCM-41 and regeneration of the sorbent using microwave digestion. *J Hazard Mater* 193:171–176. <https://doi.org/10.1016/j.jhazmat.2011.07.037>
- İlbay Z, Haşımoğlu A, Özdemir OK, Ateş F, Şahin S (2017) Highly efficient recovery of biophenols onto graphene oxide nanosheets: valorisation of a biomass. *J Mol Liq* 246:208. <https://doi.org/10.1016/j.molliq.2017.09.046>
- Kushwaha AK, Gupta N, Chattopadhyaya MC (2014a) Enhanced adsorption of methylene blue on modified silica gel: equilibrium, kinetic, and thermodynamic studies. *Desalin Water Treat* 52(22–24):4527–4537. <https://doi.org/10.1080/19443994.2013.803319>
- Kushwaha AK, Gupta N, Chattopadhyaya MC (2014b) Enhanced adsorption of methylene blue on modified silica gel: equilibrium, kinetic, and thermodynamic studies. *Desalin Water Treat* 52(22–24):4527–4537. <https://doi.org/10.1080/19443994.2013.803319>
- Lu T, Ten Hagen TL (2020) A novel kinetic model to describe the ultrafast triggered release of thermosensitive liposomal drug delivery systems. *J Control Release* 324:669. <https://doi.org/10.1016/j.jconrel.2020.05.047>
- Mahmoudi J, Lotfollahi MN, Asl AH (2015) Comparison of synthesized H-Al-MCM-41 with different Si/Al ratios for benzene reduction in gasoline with propylene. *J Ind Eng Chem* 24:113–120. <https://doi.org/10.1016/j.jiec.2014.09.017>
- Mannaa MA, Altass HM, Salama RS (2021) MCM-41 grafted with citric acid: The role of carboxylic groups in enhancing the synthesis of xanthenes and removal of heavy metal ions. *Environ*

- Nanotechnol Monit Manag 15:100410. <https://doi.org/10.1016/j.enmm.2020.100410>
- Manzano M, Vallet-Regí M (2010) New developments in ordered mesoporous materials for drug delivery. *J Mater Chem* 20(27):5593–5604. <https://doi.org/10.1039/B922651F>
- Monash P, Pugazhenthí G (2010) Investigation of equilibrium and kinetic parameters of methylene blue adsorption onto MCM-41. *Korean J Chem Eng* 27(4):1184–1191. <https://doi.org/10.1007/s11814-010-0177-8>
- Musial W, Kokol V, Voncina B (2010) Deposition and release of chlorhexidine from non-ionic and anionic polymer matrices. *Chem Pap* 64(3):346–353. <https://doi.org/10.2478/s11696-010-0013-y>
- Parida K, Mishra KG, Dash SK (2012) Adsorption of copper (II) on NH₂-MCM-41 and its application for epoxidation of styrene. *Ind Eng Chem Res* 51(5):2235–2246. <https://doi.org/10.1021/ie200109h>
- Pasandideh Z, Tajabadi M, Javadvpour J, Mirkazemi SM (2020) The effects of Fe³⁺ and Co²⁺ substitution in Ca_{10-x-y}Fe_xCo_y(PO₄)₆(OH)₂ hydroxyapatite nanoparticles: magnetic, antibacterial, and improved drug release behavior. *Ceram Int* 46(10):16104. <https://doi.org/10.1016/j.ceramint.2020.03.163>
- Popova T, Tzankov B, Voycheva C, Spassova I, Kovacheva D, Tzankov S, Lambov N (2021) Mesoporous silica MCM-41 and HMS as advanced drug delivery carriers for bicalutamide. *J Drug Deliv Sci Technol* 62:102340. <https://doi.org/10.1016/j.jddst.2021.102340>
- Rafati L, Ehrampoush MH, Rafati AA, Mokhtari M, Mahvi AH (2016) Modeling of adsorption kinetic and equilibrium isotherms of naproxen onto functionalized nano-clay composite adsorbent. *J Mol Liq* 224:832. <https://doi.org/10.1016/j.molliq.2016.10.059>
- Soenmez M, Fıcaı D, Fıcaı A, Alexandrescu L, Georgescu M, Trusca R, Andronescu E (2018) Applications of mesoporous silica in biosensing and controlled release of insulin. *Int J Pharm* 549(1–2):179. <https://doi.org/10.1016/j.ijpharm.2018.07.037>
- Solanki P, Patel S, Devkar R, Patel A (2019) Camptothecin encapsulated into functionalized MCM-41: in vitro release study, cytotoxicity and kinetics. *Mater Sci Eng C* 98:1014–1021. <https://doi.org/10.1016/j.msec.2019.01.065>
- Talaei M, Hassanzadeh-Tabrizi SA, Saffar-Teluri A (2021) Synthesis of mesoporous CuFe₂O₄@ SiO₂ core-shell nanocomposite for simultaneous drug release and hyperthermia applications. *Ceram Int* 47(21):30287. <https://doi.org/10.1016/j.ceramint.2021.07.209>
- Vidyadhara S, Babu JR, Balakrishna T, Trilochani P, Kumar MP (2013) Design and evaluation of controlled release losartan potassium microcapsules. *J Pharm Res* 6(4):470–475. <https://doi.org/10.1016/j.jopr.2013.04.015>
- Vilaça N, Amorim R, Machado AF, Parpot P, Pereira MF, Sardo M, Baltazar F (2013) Potentiation of 5-fluorouracil encapsulated in zeolites as drug delivery systems for in vitro models of colorectal carcinoma. *Colloids Surf B Biointerfaces* 112(2013):237–244. <https://doi.org/10.1016/j.colsurfb.2013.07.042>
- Wang S (2009) Ordered mesoporous materials for drug delivery. *Microporous Mesoporous Mater* 117(1–2):1–9. <https://doi.org/10.1016/j.micromeso.2008.07.002>
- Zendehdel M, Cruciani G, Kar FS, Barati A (2014) Synthesis and study the controlled release of etonidazole from the new PEG/NaY and PEG/MCM-41 nanocomposites. *J Environ Health Sci Eng* 12(1):35. <https://doi.org/10.1186/2052-336X-12-35>

Publisher's Note Springer Nature remains neutral with regard to jurisdictional claims in published maps and institutional affiliations.